Applied Energy 191 (2017) 568–581

Contents lists available at ScienceDirect

Applied Energy

journal homepage: www.elsevier.com/locate/apenergy

The effect of cylinder liner operating temperature on frictional loss and engine emissions in piston ring conjunction

R. Rahmani [a,*], H. Rahnejat [a], B. Fitzsimons [b], D. Dowson [a]

[a] Wolfson School of Mechanical & Manufacturing Engineering, Loughborough University, Loughborough, Leicestershire, UK
[b] Aston Martin Lagonda Ltd., Gaydon, Warwickshire, UK

HIGHLIGHTS

- Cylinder liner temperature affects frictional losses.
- Optimum liner temperature improves energy efficiency and reduces emissions.
- Liner temperature is hardly affected by viscous shear of lubricant.
- This implies optimum conditions would be independent of engine speed.

ARTICLE INFO

Article history:
Received 24 June 2016
Received in revised form 19 December 2016
Accepted 27 January 2017

Keywords:
Internal Combustion (IC) engine
Cylinder liner
Piston ring
Friction
Friction Mean Effective Pressure (FMEP)
Energy loss
Fuel consumption

ABSTRACT

Despite extensive research into alternative methods, the internal combustion engine is expected to remain as the primary source of vehicular propulsion for the foreseeable future. There are still significant opportunities for improving fuel efficiency, thus directly reducing the harmful emissions. Consequently, mitigation of thermal and frictional losses has gradually become a priority. The piston-cylinder system accounts for the major share of all the losses as well as emissions. Therefore, the need for an integrated approach, particularly of a predictive nature is essential. This paper addresses this issue, particularly the role of cylinder liner temperature, which affects both thermal and frictional performance of the piston-cylinder system. The study focuses on the top compression ring whose critical sealing function makes it a major source of frictional power loss and a critical component in guarding against further blow-by of harmful gasses. Such an integrated approach has not hitherto been reported in literature. The study shows that the cylinder liner temperature is critical in mitigating power loss as well as reducing Hydrocarbon (HC) and Nitrogen Oxide (NOx) emissions from the compression ring – cylinder liner conjunction. The results imply the existence of an optimum range for liner working temperature, independent of engine speed (at least in the studied cases) to minimise frictional losses. Combined with the study of NOx and HC emissions, the control of liner temperature can help to mitigate frictional power loss and reduce emissions.

1. Introduction

There are three main elements when optimising the performance of Internal Combustion (IC) engines in terms of improved energy efficiency. Firstly, it is important to reduce the thermal losses, which according to Richardson [1] account for 50–60% of all the losses. Secondly, frictional and pumping losses in load bearing conjunctions such as the piston-cylinder system, valve train and engine bearings represent 15–20% of all the parasitic losses. Nearly 45% of these losses can be attributed to the cylinder system, 30–45% of which is due to the ring-pack [1]. Therefore, the parasitic losses of the cylinder system account for 4–7% of the total fuel energy [1–3]. The main reason for low efficiency of engine powertrain systems is the non-optimal management of the energy conversion chain and subsequent dissipations [4]. Mitigating the sources of energy losses would improve fuel efficiency, which is a key driver in modern engine development. Finally, reducing emissions such as HC, NOx and particulates is also essential because of the environmental health issues, subject to a growing list of mandatory regulations and directives. These three aspects are increasingly and extensively studied.

To reduce the thermal losses, ideally the cylinder wall temperature should be maintained close to that of the in-cylinder gasses.

* Corresponding author.
E-mail address: R.Rahmani@lboro.ac.uk (R. Rahmani).

http://dx.doi.org/10.1016/j.apenergy.2017.01.098
0306-2619/

Nomenclature

A	contact area
A_c	surface area of combustion chamber
b	ring face (and back) width
D	bore diameter
E	Young's modulus of elasticity
E_f	Released fuel energy
E	energy
E'	composite Young's modulus of elasticity $(\frac{1}{E'} = \frac{1-\upsilon_1^2}{E_1} + \frac{1-\upsilon_2^2}{E_2})$
F	force
F_2, $F_{5/2}$	statistical functions
G	ring end gap
h	film profile
h_m	minimum film thickness
h_t	convection heat transfer coefficient
I	second moment of inertia for the ring cross-section
$\hat{i},\hat{j}$	unit vectors in x and y-directions
L	ring perimeter in the circumferential direction
l	connection rod length
m	(cylinder content) mass
m_2, m_4	the second and fourth spectral moments
$\dot{m}$	lubricant mass flow rate
N	engine speed in rpm
p	hydrodynamic pressure
P	power
Q	heat
$\dot{Q}$	heat transfer rate
R	specific gas constant
r	crank pin radius
S	compression ring face profile
s	engine stroke
T	temperature
t	time
$\underline{u}$	velocity profile
$\overline{V}$	velocity vector
V	instantaneous volume of combustion chamber
V_c	clearance volume
V_d	displaced cylinder volume
W	carried load
x,y,z	Cartesian coordinates

Greek symbols

α	pressure-viscosity coefficient
β	thermal coefficient of expansion
γ	pressure relaxation factor
Δ	ring/liner gap due to thermoelasodyncamic deformations
ΔU	sliding speed
δ	local Hertzian/EHL deformation
ζ	asperity peak density
η	lubricant dynamic viscosity
κ	average asperity tip radius of curvature
λ	Stribeck film ratio parameter
ξ	damping coefficient
ρ	lubricant density
σ	composite standard deviation of roughness $(\sigma = \sqrt{\sigma_1^2 + \sigma_2^2})$
ς	coefficient for boundary shear of asperities
τ	shear stress
υ	Poisson ratio
τ_0	Eyring shear stress
φ	crank angle
ω	engine speed

Superscripts

^{c}	composite
^{n}	iteration step

Subscripts

$_0$	ambient (atmospheric) conditions
$_{1,2}$	liner and ring
$_a$	asperity
$_{avg}$	average
$_b$	boundary
$_c$	cycle
$_e$	elastic
$_f$	fuel
$_g$	gas
$_{i,j}$	related to each computational node
$_l$	losses
$_m$	minimum
$_t$	total
$_v$	viscous
$_w$	wall

Abbreviations

BDC	Bottom Dead Centre
CFD	Computational Fluid Dynamics
DP	Detonation Point
EGR	Exhaust Gas Recirculation
FMEP	Friction Mean Effective Pressure
HC	Hydrocarbon (emissions)
IC	Internal Combustion
LHV	Lower Heating Value
MOFT	Minimum Oil Film Thickness
NEDC	New European Drive Cycle
NOx	Nitrogen-Oxides (emissions)
PSOR	Point Successive Over-Relaxation
TDC	Top Dead Centre

To a large extent, the cylinder wall temperature also determines the lubricant temperature in the contact of the top compression ring rather than any small rise due to the viscous shear heating of the lubricant in short transit times. This is shown by a recent analytical control volume, thermal mixing model by Morris et al. [5]. However, there are material and other economical cost limitations affecting the maximum attainable temperature of the cylinder liner. Cast iron and aluminium liners can operate with surface temperatures of 200–450 °C [6]. Materials with lower thermal conductivity can operate at higher temperatures. However, usually cost implications impose a practical limit on the use of such expensive liner materials, except for the limited case of race engines. In addition, the heat transfer from the hot cylinder wall to the incoming air-fuel mixture prevents the use of some materials for spark ignition (SI) engines [6]. Furthermore, the above set of ideals cannot be assured under cold start-up conditions or with intermittent stop-start and other transient driving conditions, which are progressively prevalent.

With regard to the emission levels, Wang and Stone [7] showed that the cylinder wall temperature is a significant parameter influencing HC and NOx emissions from IC engines. It was shown that the HC emissions tend to reduce with a higher liner temperature, whilst the contrary is usually true of NOx emissions. Therefore, an optimum liner temperature should be sought, based upon a

desired (weighted) trade-off between the HC and NOx emissions. In addition, it is shown that technologies such as EGR can mitigate the NOx formation particularly at high loads. However, this has a detrimental effect on the tribology of the engine and other types of emission [8].

Cylinder liner temperature has a significant role in thermodynamic control-oriented modelling of cycle-to-cycle exhaust gas temperature. Dehghani Firoozabadi et al. [9] have highlighted the importance of defining the cylinder wall temperature as a function of engine loading and coolant temperature to improve such models. Furthermore, according to Razmara et al. [10], optimal control of IC engines both in transient and steady-state operation can be achieved through an availability or exergy-based analysis. Such an approach considers main sources of exergy losses, including combustion irreversibility, heat loss and frictional losses. This control approach can potentially lead to about 6–7% saving in fuel consumption compared with other more conventional control methods.

The current paper attempts to address the issue of frictional losses particularly in the top compression ring-cylinder liner conjunction, which accounts for 1–3% of the fuel consumption [1]. This is mainly due to the requirement for good circumferential conformity of the ring to the cylinder liner surface in order to ensure its primary function of sealing the combustion chamber. The study demonstrates the effect of liner temperature on the frictional losses of this conjunction.

The sealing function of the compression ring needs to be retained to guard against loss of power and ingression of combustion by-products into the bottom end of the engine. Effective sealing has the drawback of increased friction. Therefore, improvement of tribological performance of the compression ring poses a significant challenge. One reason for this is the plethora of interacting parameters which need to be addressed simultaneously. These include the ring's contact face-width geometry and its surface topography [11], mechanical and thermal properties of any hard wear-resistant coating, ring's elastodynamics [12,13] and the lubricant rheological properties, as well as the influence of various lubricant additives. This list of parameters is not exhaustive, thus making the full analysis very complex. For this reason, many researchers have focused on particular tribological phenomena. For instance, Arcoumanis et al. [14], Han and Lee [15], Priest et al. [16], Sawicki and Yu [17] and Shahmohamadi et al. [18] have paid particular attention to various lubricant cavitation models. This affects the load carrying capacity of the conjunction as well as the generated friction and heat transfer. Hu et al. [19], Ma et al. [20] and Rahmani et al. [21] studied the ring-liner conjunction with an emphasis on bore circumferential out-of-roundness, distortion and the ability of the ring to conform to such distorted geometries. The effect of surface topography has also been studied by Michail and Barber [22,23], Bolander et al. [24,25] and Morris et al. [11]. Although many important findings have emerged from these studies, they mostly relate to assumed isothermal conditions, except for Morris et al. [5] and Ma et al. [26] who adjusted the lubricant temperature and that of the liner surface.

Richardson and Borman [27] reported a combined numerical-experimental investigation of boundary conditions using a reciprocating test rig, as well as a motored engine to study the effect of lubricant temperature due to viscous shear heating at different sliding speeds for different lubricants. The results showed that although at a lower liner temperature of 40 °C and speed of 2000 rpm a rise of about 5–10 °C was noted, at higher surface temperatures (100 °C and above) the viscous shear heating accounted for less than 2 °C. This finding is in accord with the combined solution of Reynolds equation and control volume analytical thermal mixing model of Morris et al. [5]. They indicate that measured liner surface temperature can be used for predictive analyses under the usual engine running conditions. Richardson and Borman [27], however, did not include the effect of variations in the liner temperature at various engine running conditions and its influence upon the ensuing frictional losses. Ma et al. [26] considered the influence of cylinder wall temperature on friction in piston ring-cylinder liner contact using a one- dimensional mixed lubrication average flow model. The variations of minimum oil film thickness and friction with the average liner surface temperature was investigated. It was shown that minimum friction occurs for liner temperatures in the range 140–150 °C, with the higher contribution being due to viscous friction. However, at the higher liner temperature range of 160–170 °C, asperity friction accounts for the main contribution to the total generated friction.

It is clear that an increase in lubricant temperature, governed in the most part by the liner surface temperature reduces the viscous friction. However, at piston reversals with a low sliding velocity, an increasing boundary friction accounts for the main contribution to friction, and there is reduced dependence on liner surface temperature. A recent study by Mufti et al. [28] has shown that the rise in power losses above a certain temperature due to asperity interactions can be quite significant. In addition, oil temperature variations interfere with the cooling fluid temperatures due to its faster dynamics [29]. Therefore, there should be an "optimum" liner working temperature for given engines to minimise the overall cyclic nature of frictional losses due to both viscous and boundary contributions. The liner temperature and subsequent implications on the engine friction is also closely related to the choice of lubricating oil grade and its additive package, which can affect, for instance, PM emissions from the engines [30]. The current study focuses on predicting such an "optimum" working liner temperature for a high performance 12-cylinder, 4-stroke naturally aspirated gasoline engine. The findings are compared with some of the aforementioned studies.

2. Theory

2.1. Pressure distribution

The pressure distribution in the ring-liner contact is obtained through solution of Reynolds equation:

$$\frac{\partial}{\partial x}\left[\left(\frac{\rho h^3}{6\eta}\right)\frac{\partial p}{\partial x}\right]+\frac{\partial}{\partial y}\left[\left(\frac{\rho h^3}{6\eta}\right)\frac{\partial p}{\partial y}\right]=\Delta U\frac{\partial}{\partial x}(\rho h)+2\frac{\partial}{\partial t}(\rho h) \quad (1)$$

It is assumed that there is no side leakage of the lubricant in the circumferential direction, and where ΔU is the piston sliding speed [31]:

$$\Delta U(\varphi)=-r\omega\sin\varphi\{1+\cos\varphi[(l/r)^2-\sin^2\varphi]^{-1/2}\} \quad (2)$$

where φ is the crank-angle, l is the connecting rod length, r the crank pin radius and ω is the engine rotational speed.

For boundary conditions, the lubricant inlet and exit pressures are set to in-cylinder and crank case pressures respectively, depending on the piston motion. The variations of in-cylinder pressure at two different engine speeds have been measured (Fig. 2), using a spark plug-type Kistler pressure transducer fitted into the combustion chamber.

2.2. Boundary conditions

Swift-Stieber exit boundary conditions have been used to determine the position of lubricant film rupture and the onset of cavitation. In the numerical solution of Reynolds equation, pressures below the lubricant vaporisation pressure are set to the cavitation pressure. This action fulfils the zero pressure gradient condition at

the lubricant rupture point as required by the Swift-Stieber conditions (Christopherson [32]). It is also assumed that the pressure throughout the cavitation region remains unaltered. However, for the lubricant to be able to exit from the conjunction, the pressure at the exit should at least be equal to the ambient pressure. In the ring upstroke motion, for example in the compression stroke, the pressure at the conjunctional exit is the measured in-cylinder pressure. Therefore, the lubricant pressure must ascend to the in-cylinder pressure at the contact exit. Elrod's reformation model can predict the rise of the lubricant pressure at the exit boundary [33]. A multi-phase solution, using Navier-Stokes, energy and vapour transport equations is provided by Shahmohamadi et al. [18]. Implementing the method outlined by Christopherson [32] ensures that the pressure at the exit becomes that of the outlet pressure, although the gradient of pressure rise from the cavitation pressure to that of the outlet pressure is different from that predicted by Elrod [33]. A further discussion on this issue is provided in Han and Lee [15].

The pressures at the ring edges in the circumferential direction are set to the ring end gap pressure which is estimated to be the average of the in-cylinder and crank case pressures.

2.3. Lubricant rheology

For lubricant density, a modified version of Dowson and Higginson [34] relationship is used, to include the effect of temperature (Yang et al. [35]):

$$\rho = \rho_0\left[1+\frac{0.6\times10^{-9}(p-p_0)}{1+1.7\times10^{-9}(p-p_0)}\right][1-\beta(T-T_0)] \tag{3}$$

The lubricant viscosity variation with pressure and temperature is given as [36]:

$$\eta = \eta_0\exp\left\{(\ln\eta_0+9.67)\left[\left(\frac{T-138}{T_0-138}\right)^{\frac{\beta_0(T_0-138)}{\ln\eta_0+9.67}}\times\left(1+\frac{p-p_0}{1.98\times10^8}\right)^{\frac{1.98\times10^8\alpha_0}{\ln\eta_0+9.67}}-1\right]\right\} \tag{4}$$

The lubricant properties used in the current study are listed in Table 1.

2.4. Ring profile and film shape

The gap between the ring and the liner is in general defined as:

$$h(x,y,t) = h_m(t)+S(x)+\delta(p)+\Delta(y,t) \tag{5}$$

Due to the relatively low pressure values in the ring-liner contact (of order of a few hundred MPa) no localised deformation of the contiguous surfaces is expected (Mishra et al. [37] and Ma et al. [20]), thus: $\delta = 0$.

The variation of the ring-liner gap in the circumferential direction, Δ, is the result of its thermo-elastic distortion and/or elasto-dynamic behaviour (ring modal action). These effects are ignored in the current analysis, which are described by Tian et al. [12] and Baker et al. [13]. Additionally, in practice the bore is not an idealised right circular cylinder. This, together with the thermo-elastic distortion of the liner (Littlefair et al. [38]) affects the underformed gap between the ring and the liner. A representative analysis is reported elsewhere by Rahmani et al. [21]. The current analysis assumes an idealised circular cylindrical bore with insignificant thermo-elastic deformation, thus: $\Delta = 0$.

To reflect real working conditions, a run-in ring profile was measured using an optical Talysurf. Then, a 6th-order polynomial was fit to the measured profile (see Fig. 3).

The 6th-order polynomial fitted ring contacting profile is expressed as:

$$S(x) = -6.5x^6 - 49.8x^5 + 143.2x^4 - 98.5x^3 + 27.4x^2 - 17.3x + 7.5 \tag{6}$$

where the units of x and S are millimetres and micrometres respectively.

Table 1
Lubricant rheological properties (SAE 10W40).

Parameter	Value	Unit
Pressure-viscosity coefficient	1×10^{-8}	m^2/N
Thermal expansion coefficient	6.5×10^{-4}	K^{-1}
Density	849.7 @ 15 °C, 833.8 @ 40 °C	kg/m^3
Kinematic viscosity	59.99 @ 40 °C, 9.590 @ 100 °C	$\times10^{-6}$ m^2/s
Eyring shear stress	2.0	MPa

2.5. Surface topography and asperity interactions

A mixed lubrication regime usually occurs after $\lambda = h/\sigma < 3$. Thus, a proportion of the load is carried by the direct interaction of asperities on the counter-face surfaces. The Greenwood and Tripp [39] model is used to describe the load carried by the asperities. The underlying assumption here is that the cross-hatched surface of the cylinder liner can be assumed to embody a Gaussian distribution of asperity heights, which is not the case in practice as noted by Michail and Barber [22,23]. However, engine testing results by Gore et al. [40] have shown that after the initial running-in period, a plateau surface is achieved where the roughness on the plateau can be represented by a Gaussian distribution with its Rk value and little change in the depth of the cross-hatched valleys occur. Therefore, the present analysis represents the contact of ring with the cylinder liner plateau after running-in.

Elemental loads carried by an area of asperity tip contacts, $dA = dx.dy$ is obtained as [39]:

$$dW_a = \frac{16\sqrt{2}}{15}\pi(\zeta\kappa\sigma)^2\sqrt{\frac{\sigma}{\kappa}}E'F_{5/2}(\lambda)dA \tag{7}$$

The statistical function $F_5/_2$ is representative of an assumed Gaussian distribution of asperities in terms of λ. Since two contacting surfaces (the ring and the liner) are rough, a method described by Arcoumanis et al. [41] is used to describe the composite roughness parameters $\zeta\kappa\sigma$ (known as the Tabor's roughness parameter) and σ/κ, which is representative of the combined asperity slope [42].

The surface topography of the ring face-width and the liner were measured using the white light interferometer, Zygo. The acquired topographical data was used to obtain the second and fourth spectral moments of each surface topographical trace. These were subsequently used in the composite form, representing an equivalent rough surface contacting a smooth plane. Then, the required parameters ζ and κ are calculated as [41]:

$$\zeta = \frac{1}{6\pi\sqrt{3}}\left(\frac{m_4^c}{m_2^c}\right) \tag{8}$$

and:

$$\kappa = \frac{3\sqrt{\pi}}{8}\sqrt{\frac{1}{m_4^c}} \tag{9}$$

The results obtained from the measurements and the subsequent calculations of surface topographical parameters are listed in Table 2.

Table 2
Surface topographical parameters for ring and liner after running-in.

Parameter	Value	Unit
σ_1 for liner	0.260	μm
σ_2 for ring	0.235	μm
$(\zeta\kappa\sigma)^c$ for (combined) ring and liner	0.065	–
$(\sigma/\kappa)^c$ for (combined) ring and liner	0.192	–

2.6. Load carrying capacity

The total load carrying capacity (contact reaction) is obtained by summing the contributions due to hydrodynamic pressures and asperity interactions as:

$$W_t = \int_0^L \int_0^b (dW_a + p)dxdy \tag{10}$$

Ignoring any loading due to the ring's inertial radial motion, the contact reaction should instantaneously balance the applied load on the ring-liner contact as the result of ring fitment (ring tension) and gas pressure loading [21]. The gas pressure acts behind the inner rim of the ring. Both the gas force and the ring tension strive to press the ring to the surface of the liner. Thus:

$$F_t = F_e + F_g = \frac{8GEI}{3\pi D^3} + \int_0^L \int_0^b p_g dxdy \tag{11}$$

To calculate the exact gas pressure behind the ring, a gas blow-by model such as those developed in [26,43] is required. In the current study, it is assumed that the total combustion gas pressure acts behind the top compression ring. As the result of this assumption the chance of boundary friction contribution is increased.

2.7. Conjunctional friction and power loss

There are two contributions to the overall ring-liner friction. These are as the result of viscous shear of a lubricant film and any direct interaction of asperity tips on the counter face surfaces. Viscous friction is obtained as:

$$f_v = \int |\vec{\tau}_v| dA_v \tag{12}$$

where the viscous shear stress acting on the liner surface is:

$$\vec{\tau}_v = -\frac{h}{2}\vec{\nabla}p - \Delta\vec{V}\frac{\eta}{h} \quad \text{where, } \vec{\nabla} \equiv \left(\frac{\partial}{\partial x}\hat{i} + \frac{\partial}{\partial y}\hat{j}\right) \tag{13}$$

The elemental viscous shear contact area is:

$$dA_v = dA - dA_a \tag{14}$$

where the elemental asperity area of contact is obtained from Greenwood and Tripp [39]:

$$dA_a = \pi^2(\zeta\kappa\sigma)^2 dA F_2(\lambda) \tag{15}$$

The boundary friction force is expressed as:

$$f_b = \tau_0 A_a + \varsigma W_a \tag{16}$$

Eq. (16) assumes that the asperities are wetted by adsorption of an ultra-thin film of boundary active molecules within the lubricant. Briscoe and Evans [44] assume that a thin adsorbed film of boundary active lubricant species is subject to non-Newtonian shear. This non-Newtonian shear behaviour commences at the Eyring shear stress of the lubricant; τ_0.

The statistical function $F_2(\lambda)$ is representative of an assumed Gaussian distribution of asperities in terms of λ [39]. Various values for the pressure coefficient of boundary shear of asperities, ς are used in the literature. This parameter is closely related to the surface material and topographical properties. For the employed ring in the current study a specific value for the pressure coefficient of boundary shear strength of asperities is obtained as $\varsigma = 0.14$ through use of atomic force microscopy in lateral force mode as described by Styles et al. [45].

The total power loss at each crank angle is therefore, obtained as:

$$P_l = (f_v + f_b)\Delta U \tag{17}$$

The top ring Friction Mean Effective Pressure (FMEP) can also be calculated as follows (Sui and Ariga [46]):

$$FMEP = \frac{\int P_l dt}{V_d} \tag{18}$$

where the cylinder swept volume is:

$$V_d = \frac{\pi}{4}D^2 sN \tag{19}$$

In addition, the lubricant mass flow rate in the axial entrainment direction and at any cross-section is obtained as:

$$\dot{m} = \int_0^L \int_0^h u dz\, dy = \left[-\frac{h^3}{12\eta}\left(\frac{\partial p}{\partial x}\right) + \frac{(U_1+U_2)h}{2}\right]L \quad \text{where, } L = \pi D \tag{20}$$

3. Method of solution

To obtain the pressure distribution, Reynolds equation (1), lubricant rheological state Eqs. (3) and (4) and the film shape (5) are solved simultaneously by iteration. Appendix A provides the details of the discretised equation. Pressure at any computational node is obtained through finite difference Point Successive Over-Relaxation (PSOR) iterative method described by Hoffmann and Chiang [47]. PSOR is a variant of general Successive Over-Relaxation (SOR) methods. It is principally a variant of the Gauss-Seidel iterative method for solving a linear system of equations which results in faster convergence. In this method, at each iteration step, the data at each computational grid point is updated by using more than 100% of the newly obtained data for that point (over-relaxation). This is unlike the under-relaxation methods, where a percentage of the newly obtained data for each grid point is taken to the next iteration, which adds to the computational time. The pressure for each node is updated using an under/over-relaxation method:

$$p_{i,j}^n = (1-\gamma)p_{i,j}^{n-1} + \gamma p_{i,j}^n \quad (0 < \gamma < 2) \tag{21}$$

For the current problem an over-relaxation factor of $\gamma = 1.784$ was found to be the optimum.

Since the lubricant rheological parameters are functions of pressure, in each pressure iterative cycle, the lubricant density and viscosity are also updated accordingly.

The pressure convergence criterion is:

$$\frac{\sum_i\sum_j |p_{i,j}^n - p_{i,j}^{n-1}|}{\sum_i\sum_j p_{i,j}^n} \leqslant 1\times 10^{-5} \tag{22}$$

At any given crank angle φ, force balance on the ring is sought, using the convergence criterion:

$$\frac{|F_t(\varphi) - W_t(\varphi)|}{F_t(\varphi)} \leqslant 1\times 10^{-3} \tag{23}$$

If this criterion is not met, then the minimum film thickness is adjusted as described in [21]:

$$h_m^n = \left[1 + \xi\left(\frac{W_t(\varphi) - F_t(\varphi)}{max\{W_t(\varphi), F_t(\varphi)\}}\right)\right] h_m^{n-1} \quad (24)$$

and the entire pressure and load iterations are repeated. A damping coefficient of $\xi = 0.05$ is used to achieve faster load convergence, whilst avoiding numerical instability.

Finally, to ensure a periodic engine cycle the following condition must also be satisfied:

$$\frac{|h_m(\varphi) - h_m(\varphi - 720)|}{h_m(\varphi - 720)} \leqslant 1 \times 10^{-3} \quad (25)$$

Friction and frictional power loss is obtained after the convergence criteria are met at each step of simulation (i.e. crank angle location).

Further details on the numerical model and solution methodology can be found in [21].

4. Results and discussion

A series of simulations have been carried out, using the input data in Tables 1 and 2 and the engine operating conditions in Figs. 1 and 2. A series of results were obtained at three operating liner temperatures of 40, 80 and 120 °C. These temperatures were chosen for the simulation studies as they represent the lubricant condition in fast transit through the contact and in line with the findings of Morris et al. [11]. These engine speed-liner temperature combinations also correspond to the low speed NEDC (New European Drive Cycle), from cold running, through transient conditions (from cold start to hot cycle) and onto the hot low speed conditions, all typical of urban driving situations. The NEDC is a standard test for the evaluation of emission performance of vehicles [48]. The engine pressure measurements at both speeds are taken at 100% throttle. Considering a relatively higher idle speed for high performance engines, the conditions at full throttle and lower speed with low temperatures represent the cold start phase. At higher temperatures this will correspond to stop-start conditions typical of urban driving cycle in congested traffic. The higher speed at 100% throttle and mid to higher temperatures is intended for the transient part of the NEDC in urban driving cycle.

4.1. Friction and power loss

Fig. 4 shows the predicted variation of minimum film thickness for the studied ring profile (Fig. 3) at the engine speed of 1500 rpm and three different liner temperatures. The boundaries between various regimes of lubrication $\lambda \geqslant 3$ (hydrodynamic), $1 \leqslant \lambda < 3$ (mixed regime of lubrication) and $\lambda < 1$ (boundary regime of lubrication) are also shown in the figure. For most of the engine cycle, the ring-liner contact is predicted to operate in the hydrodynamic regime of lubrication, particularly at mid-stroke piston location during a typical 4-stroke engine cycle. However, at the higher temperature of 120 °C, the lubrication regime remains mixed during the power stroke, even at the piston mid-span position.

As the ring approaches reversals, the regime of lubrication tends to become mixed, and just after the Top Dead Centre (TDC) reversal it is dominated by direct boundary interactions, particularly at the higher liner temperatures of 80 and 120 °C. At the lower temperature of 40 °C, aside from the transition from the compression to the power stroke at the TDC, the regime of lubrication remains hydrodynamic because of the higher lubricant viscosity at a lower liner temperature. As the inset to Fig. 4 shows, overall, the dominant regime of lubrication is mixed. No instance of purely boundary regime of lubrication is encountered. Therefore, boundary contribution to friction would be as the result of wet asperity tip pair interactions as described above.

The predicted changes in the minimum film thickness at several key locations during the engine cycle are shown in Fig. 5. Each curve in Fig. 5 shows the percentage reduction in the minimum oil film thickness as the temperature increases. The percentage reduction in minimum film thickness with temperature rise from T_1 to T_2 is calculated as:

$$\%\text{Reduction in MOFT} = \left|\frac{(h_m)_{T_2} - (h_m)_{T_1}}{(h_m)_{T_1}}\right| \times 100 \quad (26)$$

Fig. 5 shows the percentage reduction in the minimum oil film thickness (MOFT) as the result of an increasing contact temperature rise at mid-compression stroke (i.e. $\varphi = -90°$) and at the TDC in transition from the compression to power stroke (i.e.

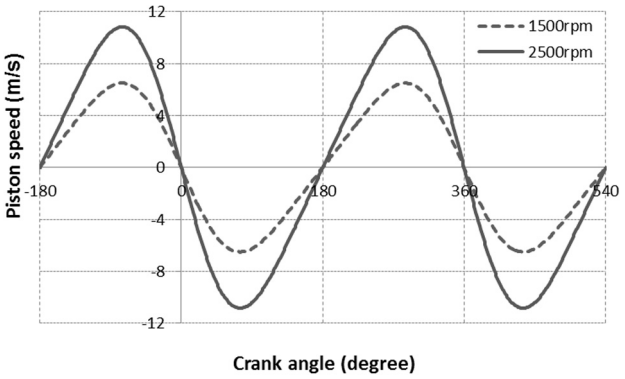

Fig. 1. Piston sliding velocity at the chosen engine speeds.

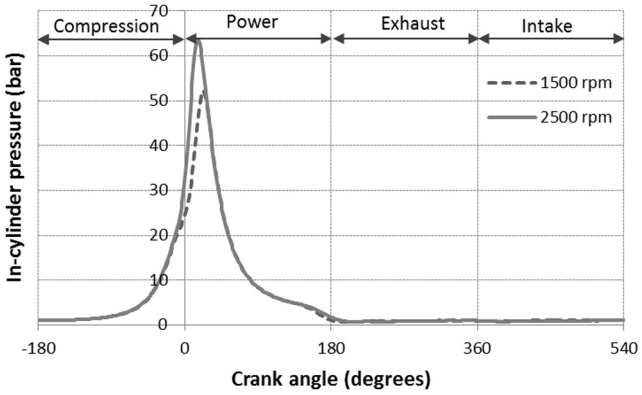

Fig. 2. In-cylinder pressure for an engine cycle at the chosen engine speeds.

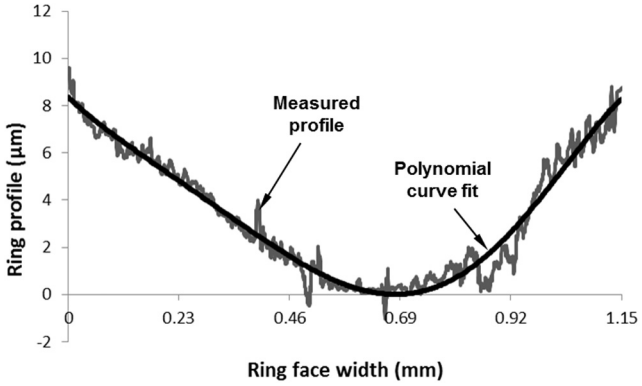

Fig. 3. Measured ring profile and polynomial fit.

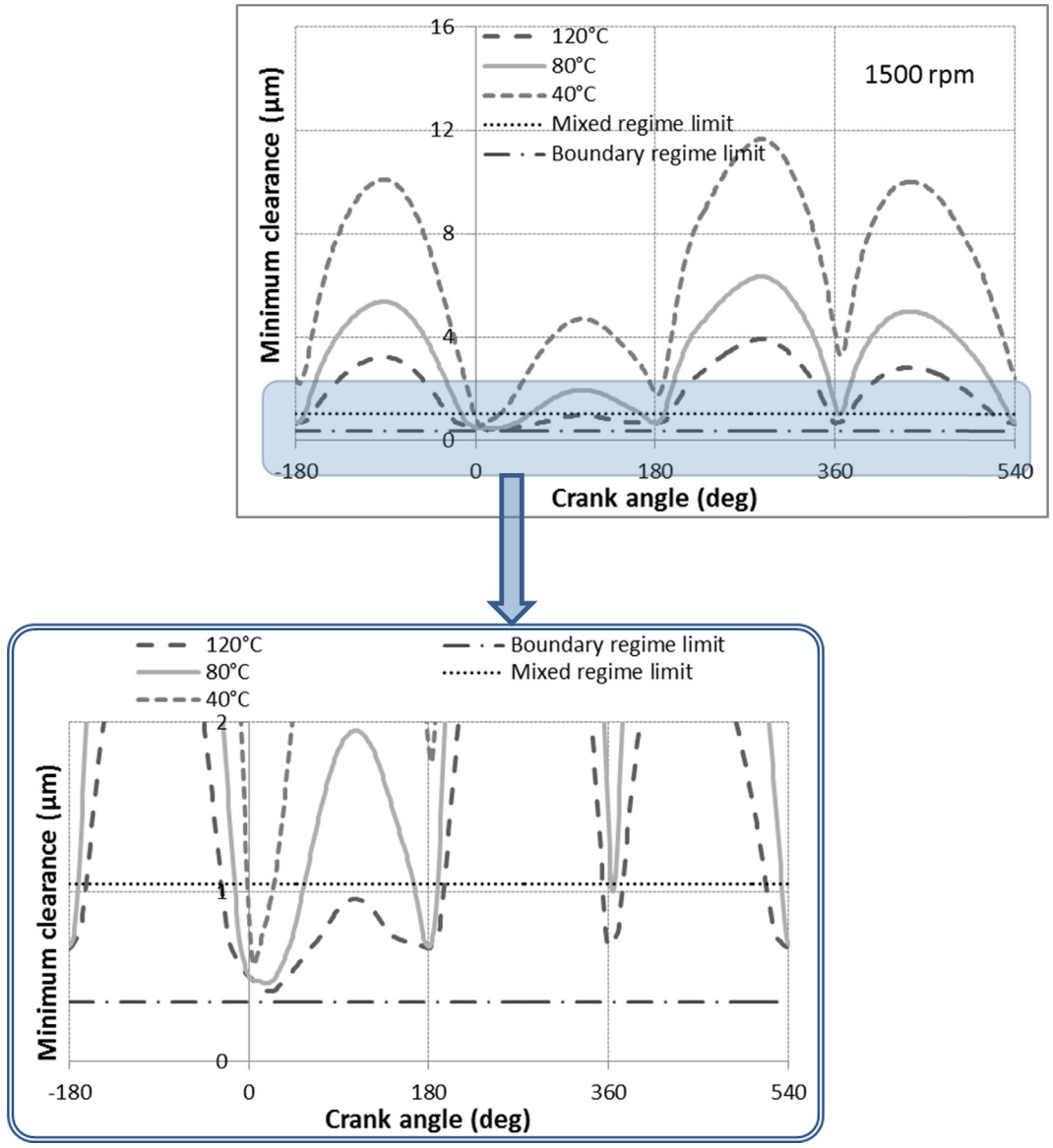

Fig. 4. Minimum film thickness variation for an engine cycle at three different liner working temperatures at engine speed of 1500 rpm.

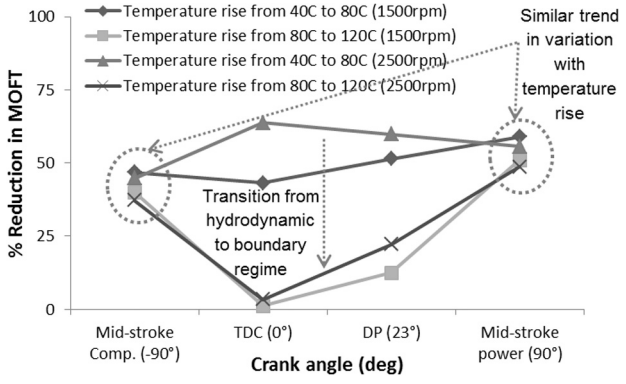

Fig. 5. Percentage reduction in minimum oil film thickness with operating temperature at different engine speeds.

$\varphi = 0°$). It also shows the same at the detonation point ($\varphi = 23°$) and finally at the mid power stroke ($\varphi = 90°$). These results are shown at both the selected engine speeds.

The results show that a 100% rise in temperature from 40 to 80 °C and a 50% temperature rise from 80 to 120 °C yield relatively similar reductions in the MOFT of about 40–55% at both mid-stroke locations ($\varphi = -90°$ and $\varphi = 90°$) for the chosen speeds. On the other hand, the minimum film thickness does not alter much with the rise in temperature from 80 to 120 °C at the TDC (i.e. $\varphi = 0°$), whereas a temperature rise from 40 to 80 °C can significantly reduce the MOFT especially at the higher speed. This suggests that as long as a hydrodynamic and to some extent a partial film prevail at the TDC, the MOFT would be quite sensitive to any variations in the liner temperature. Once the prevailing regime of lubrication tends to boundary, any variation in the lubricant temperature has virtually no effect upon the MOFT. The variation in film thickness at the Detonation Point (DP) corresponding to $\varphi = 23°$ depends upon the regime of lubrication there.

The results shown in Fig. 5 indicate that higher minimum film thickness values can be observed at lower temperatures for most of the engine cycle. This is attributed to the higher lubricant viscosity at lower temperatures. Since the same contact load is supported at each crank angle for all the three operating temperatures, then under a purely hydrodynamic regime of lubrication thinner films

would result. Therefore, working at higher temperatures would be beneficial from the oil transport perspective, as well as reduced viscous friction (lower viscosity). This can also help in reducing the amount of lubricant evaporated from the cylinder liner surface. However, at the same time this approach may affect the heat transfer from the combustion chamber to the cylinder wall and marginally increase the direct boundary interactions. Consequently, a trade-off between oil evaporation/consumption, heat transfer and increased friction due to asperity contact should be sought.

The predicted and observed reduction in the minimum oil film thickness at mid-stroke, associated with the rise in oil and liner temperature, from the current study and those reported in open literature [20,26,49] are shown in Fig. 6. It is noted that since the results are for different engines at different working conditions, the comparison only focuses on the varying trends rather than a quantitative comparison. It can be seen that the general trend is very similar in all these cases. It can also be concluded that after a certain rise in temperature, the reduction in the minimum film thickness becomes insignificant. This would occur when the prevailing regime of lubrication is mixed.

Fig. 7 provides a comparison for the lubricant mass flow rate from the ring mid-cross-section at the three studied temperatures for two different engine speeds. The reduction in oil flow rate with increasing liner temperature seems to be independent of the engine speed. For instance, an increase in the temperature from 40 to 80 °C reduces the flow rate by around 50% at both 1500 and 2500 rpm engine speeds. Additionally, a 50% increase in the working temperature from 80 to 120 °C reduces the flow rate by 42% at both these speeds.

A closer examination shows that the mass flow rate is more sensitive to the variation in the engine speed under hot working conditions. This is shown in Fig. 8, where a rising mass flow rate is predicted with an increasing engine speed at higher operating temperatures. It is also interesting to note that a 67% increase in engine speed causes a twofold rise in the lubricant flow rate at all studied working temperatures.

If hydrodynamic conditions were to prevail with an increasing engine speed at any given temperature, the increased lubricant flow rate should comply with the ratio of sliding speeds (the tested engine speeds) which is 1.67. Therefore, a progressive increase in the flow rate with temperature indicates improved lubricant availability to enhance hydrodynamic lubrication, but may result in an increased oil loss.

Fig. 9 shows the variations in the generated total friction (viscous and boundary) during the entire 4-stroke engine cycle at

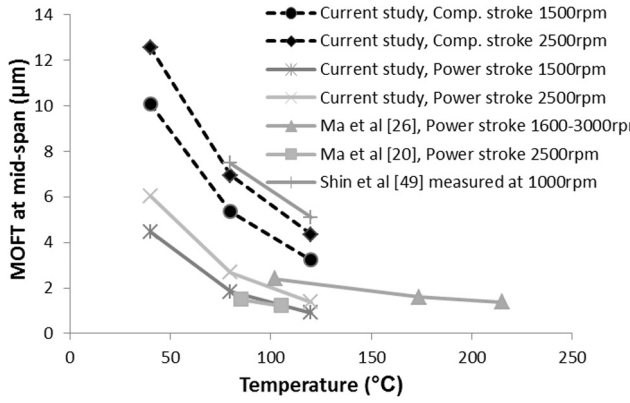

Fig. 6. Predicted and measured reduction in minimum oil film thickness at mid-span with rising operating temperature at different engine speeds.

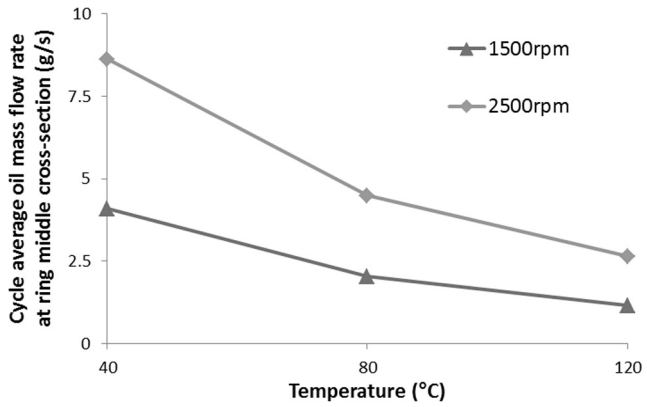

Fig. 7. Cyclic average lubricant mass flow rate at ring mid cross-section for three different liner temperatures and selected engine speeds.

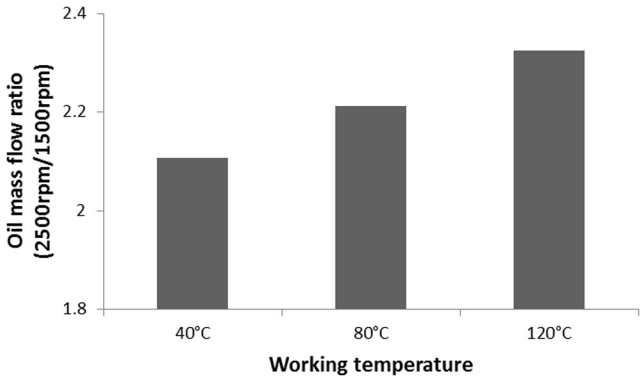

Fig. 8. Ratio of lubricant mass flow rate at the ring mid cross-section at 2500 rpm to that at 1500 rpm at three different liner temperatures.

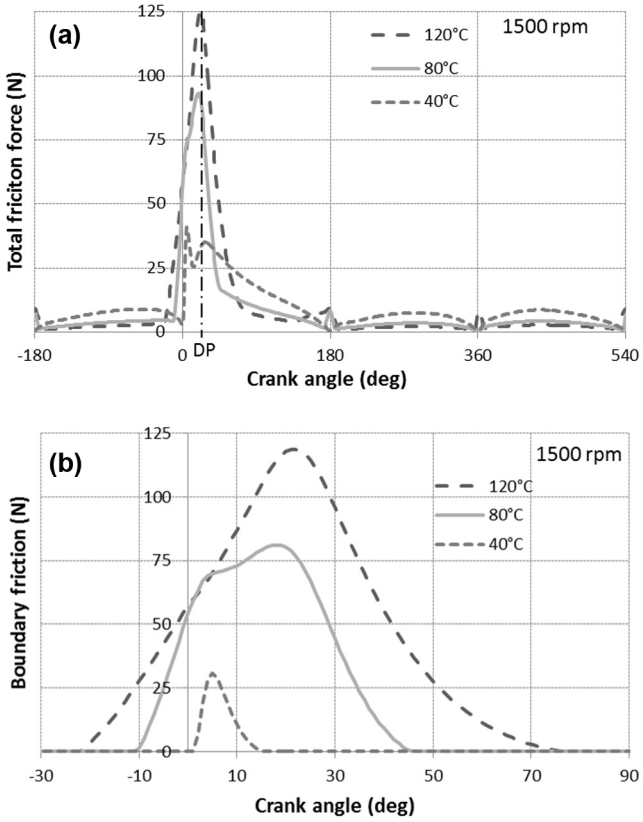

Fig. 9. Variations of (a) total friction for an engine cycle and (b) boundary friction in transition from compression to power strokes at three different working temperatures and at 1500 rpm.

the engine speed of 1500 rpm and for all the three studied liner working temperatures. Fig. 9(a) shows that the total friction is higher during the power stroke at all the three studied temperature.

The maximum total friction occurs in the power stroke between the positions of piston reversal and the mid-span with high-peaks around the Detonation Point (DP) (Fig. 9a). This is because of the higher applied pressures in this region. The position of maximum friction differs according to the engine speed and the liner working temperature, which also affects the film thickness and the lubricant viscosity. In short, it is a function of viscous shear (Poiseuille and Couette contributions) as well as some elements of boundary friction shown in Fig. 9(b).

Table 3 lists the extent of boundary friction contribution and the total friction predicted for the engine speed of 1500 rpm with different liner working temperatures.

From the results of Fig. 9, it is clear that after the maximum combustion pressure, friction dramatically reduces for the higher liner temperatures. In fact, after the crank angle of 30°, the effect of viscous shear becomes dominant. At around mid-span in the power stroke, friction for the working temperature of 120 °C is the lowest of all the investigated conditions. This is the zone in which the viscous friction is dominant and thus with the higher temperature, lower viscous shear stress and subsequently lower viscous friction would be expected.

Fig. 10 compares the cycle average viscous, boundary and total friction for the three studied operating liner temperatures and at two chosen engine speeds. At the lower temperature of 40 °C (representing cold NEDC) there is little contribution due to boundary friction, mainly on the account of higher lubricant viscosity, and thus higher load carrying capacity. The contrary is true at the high liner temperature of 120 °C. In addition, a linear relation between the boundary friction and temperature is observed. Overall, the boundary friction remains higher for the lower speed of 1500 rpm at all temperatures, clearly because of lower speed of entraining motion of the lubricant into the contact. Viscous friction is higher for engine running at the higher speed of 2500 rpm because of a higher shear rate, although the difference in viscous shear diminishes between the two engine speeds as the liner temperature rises. This clearly indicates that the lubricant viscosity plays a significant role. The variation of total friction is an amalgamation of these two mechanisms of generated friction (viscous shear of the lubricant and boundary interactions). Therefore, an optimum cycle average total friction condition at each engine speed can be identified in the figure. This trend is the same as that predicted by Ma et al. [26], also shown in Fig. 10, but clearly for a different engine and operating conditions. The prevalence of boundary friction at lower temperatures, compared with the results in [26] can be attributed to the overestimation of the contact load in the current study, where it is assumed that the pressure loading of the ring is assumed to be due to the entire combustion pressure. Use of a gas blow-by model such as that in [26,43] can alleviate this problem.

The frictional power loss from the piston compression ring in a complete engine cycle is shown in Fig. 11. A sharp rise in power loss occurs following the rise in combustion chamber pressure just after the TDC reversal (at the crank angle of 0°), and particularly at the higher liner temperatures. There is also a higher rise with increasing engine speed as well as a greater boundary contribution in this region as already described above. The dominance of losses in this region of the engine cycle provides an opportunity for some palliative measures such as localised surface texturing of liners in order to reduce the effect of boundary friction [45].

The crank angles at which the peak power loss occurs as well as its corresponding value are listed in Table 4.

Fig. 12 compares the cyclic average power loss for two engine speeds at three studied liner operating temperatures. At the operating temperature of 80 °C the minimum power loss occurs for both the studied engine speeds. In addition, despite the high peak power loss at higher temperatures (Fig. 11), Fig. 12 indicates that the overall cyclic average power loss is greater at the 40 °C operating temperature. This indicates the dominance of viscous friction.

A key observation from Fig. 12 is that at 80 °C and low engine speed, the power loss is 28.6% and 16.3% less than those at 40 (with

Table 3
Crank angles with boundary friction at the TDC (from compression to expansion strokes) and peak friction values.

Liner working temperature (°C)	Crank angle for start of boundary friction (°)	Crank angle for end of boundary friction (°)	Total crank angle (°)	Peak total friction (N)
120	−22	79	101	125.31
80	−10	46	56	93.15
40	1	16	15	41.02

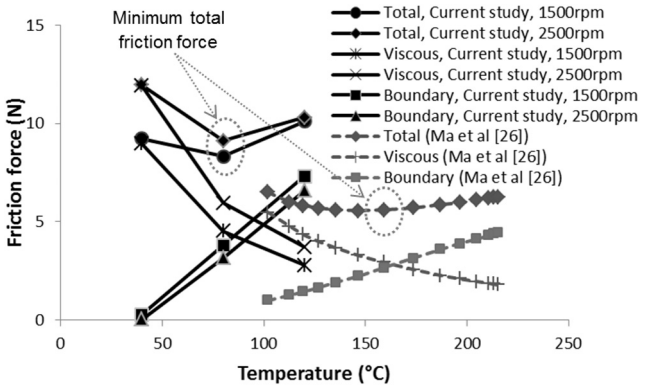

Fig. 10. Variations of predicted total, viscous and boundary friction contributions with temperature from current study and those from [26].

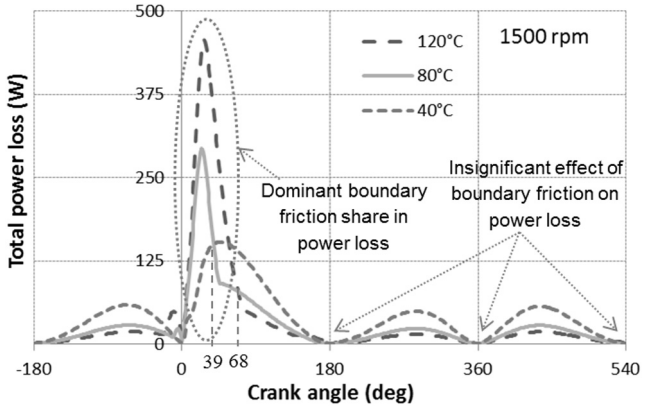

Fig. 11. Variations of power loss for an engine cycle at three different working temperatures and at 1500 rpm.

Table 4
A comparison of maximum power loss with power loss at mid-stroke during compression due to viscous shear.

Oil temperature (°C)	Crank angle for max power loss (°)	Peak power loss (W)
120	26	456.68
80	24	293.60
40	47	153.31

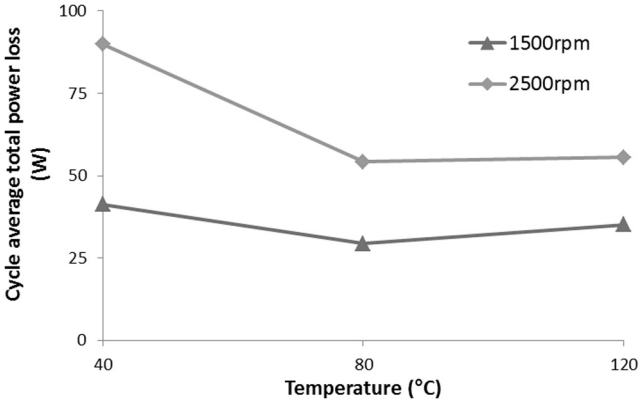

Fig. 12. Cyclic average total power loss at different liner operating temperatures and at two engine speeds.

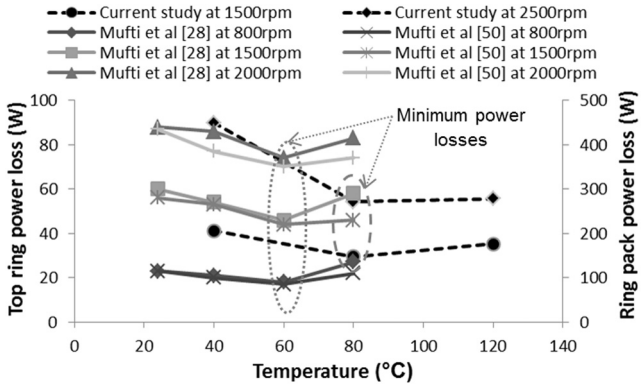

Fig. 14. Variations of predicted power loss with temperature from current study and those measured in [28,50].

higher HC) and 120 °C (with higher NOx) respectively. Therefore, the increased power loss in the cold and hot steady state conditions give rise to increased fuel consumption and harmful emissions, which is in fact the basis for the NEDC. The steady state cold and hot parts of NEDC are at low vehicle speed (low gear), corresponding to the conditions reported in the current study. Fig. 13 shows the effect of an increase of 67% in engine speeds on power loss at the 3 liner temperatures. It can be observed that an increase of twofold in power loss is predicted at 40 °C. At higher temperatures the increase in frictional losses is reduced. At 120 °C, the increase in the power loss is almost proportional to the increase in the engine speed (i.e. 58%). These conditions represent idling or low speed manoeuvres in congested traffic. The results also indicate reducing dominance of in-cycle viscous friction with an increasing liner temperature.

A comparison of variations in power loss with temperature between the current study and that of Mufti et al. [28,50] is shown in Fig. 14. The results of Mufti et al. [28,50] are for the entire piston-cylinder system (piston skirt and the ring-pack). Therefore, the aim here is only a qualitative comparison. It demonstrates that an optimum operating liner temperature may be obtained for minimum power loss. The results suggest that for all the studies shown in the figure an optimum liner temperature exists independent of the engine speed. Clearly, optimum cylinder liner temperature varies with engine operating conditions and the combustion process. Nevertheless, an implication of these findings is that the liner cooling can be controlled for the operating range of an engine in a bespoke manner in order to "optimise" the in-cycle frictional losses.

A more direct comparison with other studies for ring-liner tribological performance can be made in terms of FMEP as shown in Fig. 15, using Eq. (17). The results in Sui and Ariga [46] are for all the ring-pack, including 2 compression rings and an oil control ring. It is also based on the oil sump temperature, rather than the liner operating temperature. They showed that the lowest FMEP values occur at the highest measured temperatures and for all the engine speeds. Therefore, for the temperature range 80–100 °C, a trade-off between boundary and viscous friction for minimum FMEP was reported. Based on the results of the current study a slight rise in the FMEP may occur at higher operating temperatures, although the study of Sui and Ariga [46] did not extend to higher temperatures in order to ascertain this.

4.2. Fuel consumption

The total energy released by the combustion of fuel, E_f, in each engine cycle can be expressed as:

$$E_f = m_f Q_{LHV} \tag{27}$$

where, m_f is the mass of the input fuel injected into the combustion chamber in each cycle and Q_{LHV} is the lower calorific value of the fuel which is normally considered to be 45 MJ/kg.

The total energy lost through generated friction in the top ring-liner contact, E_l, is:

$$E_l = t_c (P_l)_{avg} \tag{28}$$

where,

$$t_c = \frac{2}{N/60} \tag{29}$$

The percentage total energy lost due to friction in the top compression ring conjunction can, therefore, be calculated using the above relations. Fig. 16 shows the percentage fuel energy loss by

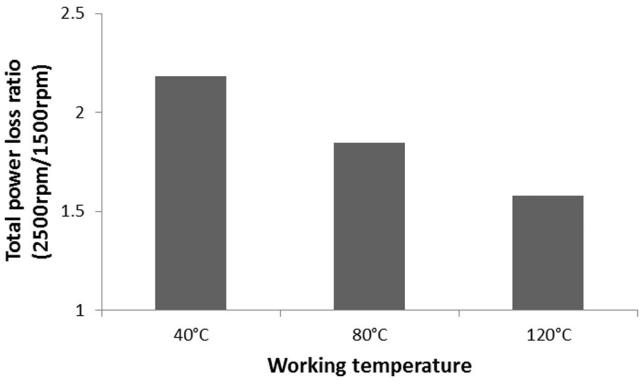

Fig. 13. Ratio of total power loss at 2500 rpm to that at 1500 rpm for different liner temperatures.

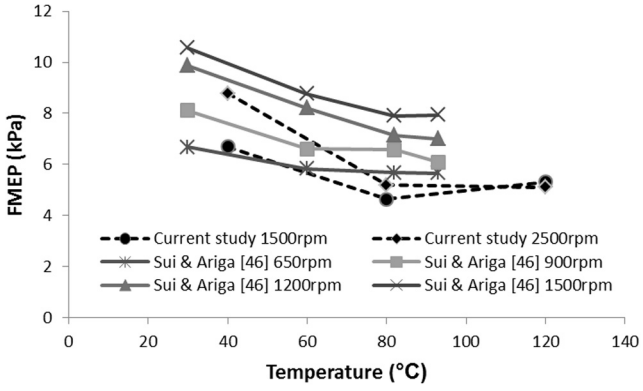

Fig. 15. Variations of FMEP with temperature from current study and those measured in [46].

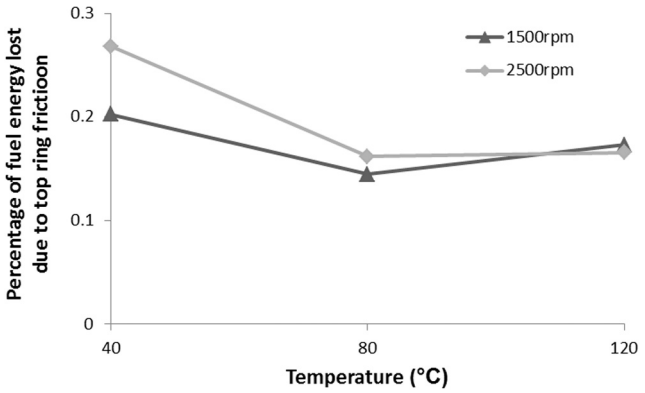

Fig. 16. Percentage input fuel energy lost due to friction of top compression ring-liner contact.

the top ring conjunctional friction at various liner temperatures and engine speeds.

It can be seen that at the liner temperature of 80 °C, the frictional energy loss is at its minimum. The reduction in fuel consumption when the operating temperature rises from 40 to 80 °C is in line with the observation made by Di Battista et al. [29], where a reduction in fuel consumption could be achieved by pre-heating the oil at the first part of the NEDC cycle.

The results also suggest that as the liner temperature rises, the effect of engine speed becomes less prominent. This is partly due to the reduced viscous friction and partly due to the reduced heat loss. For a 12-cylinder high performance engine (with the representative top compression ring as in the current study), the fuel energy loss due to the ring pack in an engine cycle is predicted to be approximately 3–4% of the input fuel, which is in line with the findings of Richardson [1].

4.3. Analysis of thermal losses

Although the main focus of this study is the effect of liner temperature upon frictional losses and fuel consumption from an IC engine, it is also interesting to investigate briefly the rate at which the thermal losses are reduced as the liner wall temperature rises. This simple method eliminates the need for a lengthy, cumbersome Computational Fluid Dynamics (CFD) and thermodynamic analyses (e.g. see [51,52]), even though such an analysis would provide more detailed and accurate predictions.

The thermal losses due to the heat transfer from the cylinder can be calculated as:

$$\dot{Q} = h_t A_c (T_g - T_w) \tag{30}$$

Using this relationship, it is possible to calculate the percentage change in the rate of thermal loss for different liner wall temperatures at any given crank angle position.

As the coefficient of convective heat transfer, surface area of combustion chamber and in-cylinder gas temperature are independent of the assumed wall temperature, the rate of heat loss at two different assumed liner wall temperatures can be obtained as:

$$\Delta\dot{Q} = \frac{\dot{Q}_2 - \dot{Q}_1}{\dot{Q}_1} = \frac{T_{w,1} - T_{w,2}}{T_g - T_{w,1}} \tag{31}$$

The gas temperature can be evaluated using the ideal gas model:

$$T_g = \frac{p_g V}{m R_g} \tag{32}$$

The variations in the in-cylinder gas pressure are shown in Fig. 2. The instantaneous volume of combustion chamber at any crank angle is:

$$V = V_c + \frac{\pi}{4} D^2 \left[l + r(1 - \cos\varphi) - (l^2 - r^2 \sin^2\varphi)^{\frac{1}{2}} \right] \tag{33}$$

In order to provide a relatively rough estimate of the cylinder wall effect on the thermal losses, a simple set of calculations can be made.

Fig. 17 shows the predicted in-cylinder gas temperature during the power stroke at two different engine speeds. It is evident that the predicted results slightly overestimate the real average gas temperature in the cylinder. This is expected due to the use of the ideal gas law as well as the assumed in-cylinder gases as air (i.e. R_g = 287 J/kg K). For simplicity, it is also assumed that the mass of the cylinder content remains constant during the entire power stroke. Despite the over-estimation, the predicted trends should not be affected, when using Eq. (31).

Using the predicted gas temperature, it is possible to calculate the reduction in the thermal losses as the liner temperature increases (Eq. (31)) as shown in Fig. 17. For instance, Fig. 18 shows the percentage reduction in the thermal losses during the power stroke for the studied engine, if the liner temperature were to rise from 70 to 80 °C.

As Fig. 18 shows the reduction has a minimum value, where the gas temperature is at its peak value (Fig. 17), when the piston is in the vicinity of the Bottom Dead Centre (BDC) and the gas temperature is reduced significantly.

The percentage average reduction in thermal loss in power stroke with a 10 °C gradual increase in the liner temperature,

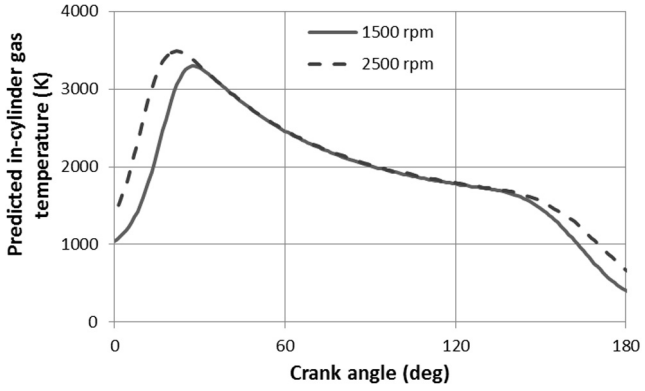

Fig. 17. Predicted in-cylinder gas temperature in the power stroke.

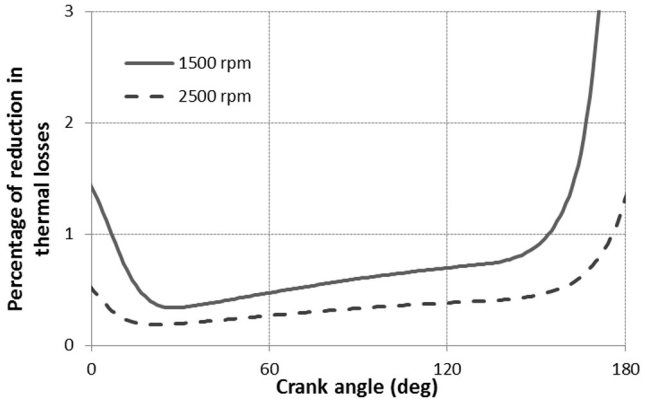

Fig. 18. Percentage reduction in thermal losses in power stroke through increasing liner surface temperature (from 70 to 80 °C).

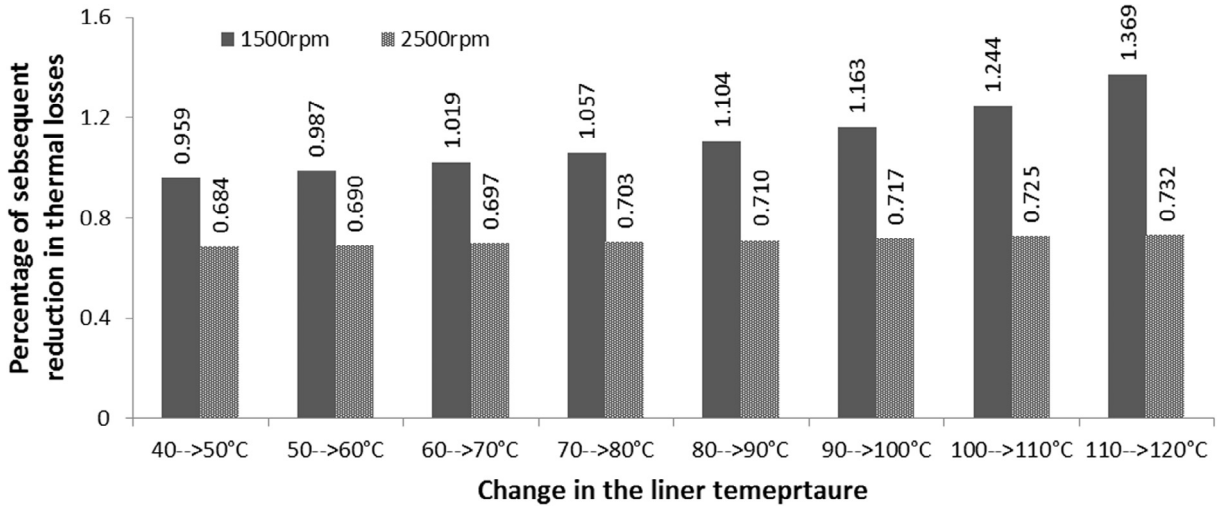

Fig. 19. Percentage average reduction in thermal losses in the power stroke for 10 °C gradual increase in liner temperature.

commencing from a start-up condition of 40 °C is shown in Fig. 19. At the lower speed of 1500 rpm an incremental rise in the liner temperature has a larger influence on the thermal losses. The results are a good indication of poorer combustion efficiency, thus increased emissions at lower temperatures, which also lead to poorer fuel efficiency as already discussed. This is the reason for the NEDC emphasis at low temperature, low speed conditions.

The results in Fig. 19 show that in general, there is no specific optimum liner temperature such as that found in the study of frictional losses. The higher the liner temperature, the lower the thermal losses and the optimum liner wall temperature is determined by other parameters such as material and thermal stress limits when only thermal losses are taken into account.

4.4. A discussion on the emissions

The current study focuses on the liner temperature effect on frictional losses from the top compression ring/liner contact. The effect of liner wall temperature on the thermal losses was also briefly discussed. The study of emissions for the current engine is also important and warrants an in-depth study of its own. A recent study by Wang and Stone [7] has specifically investigated the liner wall temperature effect on the HC and NOx emissions from an IC engine (in addition to the thermal losses) by experimental means.

Wang and Stone [7] have shown that the HC emissions reduce as the liner wall temperature rises whilst at the same time the NOx emissions increase due to rise in unburned gas temperature at the start of compression stroke which results in an increase in the maximum burned gas temperature. According to Wang and Stone [7] the rise in NOx emissions is more sensitive to liner temperature at higher loads and speeds. Therefore, a lower average liner temperature would not only reduce the total power loss from piston ring/liner contact, but it would also reduce the rate of NOx emissions, particularly at high speed and load conditions. Their results show that an optimum liner temperature exists at which, a certain trade-off between various forms of emissions can be sought.

5. Conclusions

The tribological performance of top compression ring/cylinder liner contact for a high performance V12 4-stroke naturally aspirated engine at various lubricant-liner working temperatures is studied through numerical analysis. The studied average liner temperatures correspond to conditions of the NEDC for urban driving conditions.

In general, higher minimum film thickness values are predicted for lower liner temperatures for most of the engine cycle, which is attributed to higher viscosity. It is concluded that working at higher temperature (lower lubricant viscosity) is beneficial for reducing oil transport to the combustion chamber, which can help in reducing lubricant evaporation within the chamber, thus reducing unburnt HC emissions. Consequently, a trade-off between oil evaporation (and consumption), heat transfer and increased friction and wear due to asperity interactions can be sought. The results also indicate that the existence of optimum liner working temperature, independent of engine speed (at least in the studied cases). This finding suggests that control of liner temperature can mitigate frictional power loss whilst guarding against exacerbated thermal losses. One practical implication of this finding is to operate engines at higher combustion temperatures, as this is mainly responsible for the cylinder liner operating temperature as shown by Morris et al. [5]. Many cylinder liners in high performance engines are nowadays coated with ceramic wear resistant coatings such as Diamond Like Carbon (DLC). These have poorer thermal conductivity, thus a higher operating temperature, which can suit the findings of the current study.

It is also noted that reduction in lubricant flow rate through increased liner working temperature seems to be independent of engine speed, although the oil mass flow rate itself is more sensitive to the variation in the engine speed.

These findings as well as predicting the regions of contact, where there is a greater propensity of asperity interactions, would allow prescription of localised surface treatment, such as coatings and surface texturing.

Finally, it is shown that an optimum average liner working temperature may be sought to minimise energy losses as well as emissions, particularly under urban driving conditions. Therefore, it is suggested that in the efforts made in developing control-oriented thermodynamic and emission models such as that in [53], a combined tribological analysis presented in this study with study of emissions as reported in [54] can provide a thorough understanding of the optimum engine working conditions. All three aspects of thermodynamics and heat transfer, adverse emissions and mechanical frictional losses are incorporated in the current study with their complex interactions, an approach not hitherto reported in literature.

Acknowledgments

The authors would like to express their gratitude to the Engineering and Physical Sciences Research Council (EPSRC) for the

funding of the Encyclopaedic Program Grant (www.Encyclopaedic.org), under which this research is carried out in collaboration with a consortium of industry and academic institutions. Thanks are particularly due to Aston Martin for financial and technical support of this research.

Appendix A

Eq. (1) is solved numerically using finite difference method. Using point Gauss-Seidel iteration method, the pressure at each computation node is obtained from

$$p_{i,j} = \frac{A_{i,j} + Q_{i,j}\left[(\partial p/\partial x)^2 + (\partial p/\partial y)^2\right] + 3M_{i,j}(\partial p/\partial x) - 6R_{i,j}}{2\left(\frac{1}{\Delta x^2} + \frac{1}{\Delta y^2}\right)} \quad (A.1)$$

where the pressure gradients are given by:

$$\frac{\partial p}{\partial x} = \frac{p_{i+1,j} - p_{i-1,j}}{2\Delta x} \text{ and } \frac{\partial p}{\partial y} = \frac{p_{i,j+1} - p_{i,j-1}}{2\Delta y} \quad (A.2)$$

The intermediate variables A, Q, M and R, are given by:

$$A_{i,j} = \frac{p_{i-1,j} + p_{i+1,j}}{\Delta x^2} + \frac{p_{i,j-1} + p_{i,j+1}}{\Delta y^2} \quad (A.3)$$

$$Q_{i,j} = \left[\frac{1}{\rho}\left(\frac{\partial \rho}{\partial p}\right) - \frac{1}{\eta}\frac{\partial \eta}{\partial p}\right]_{i,j} \quad (A.4)$$

$$M_{i,j} = \left[\frac{1}{h}\frac{\partial h}{\partial x} - 2\Delta U\frac{\eta}{h^2}\left(\frac{\partial \rho}{\partial p}\right)\right]_{i,j} \quad (A.5)$$

$$R_{i,j} = \left\{\frac{\eta}{h^2}\left[\left(U\frac{\partial h}{\partial x}\right) + 2\left(\frac{1}{\rho}\frac{\partial \rho}{\partial t} + \frac{1}{h}\frac{\partial h}{\partial t}\right)\right]\right\}_{i,j} \quad (A.6)$$

References

[1] Richardson DE. Review of power cylinder friction for diesel engines. Trans ASME, J Eng Gas Turb Power 2000;122:504–19.
[2] Taylor CM. Fluid-film lubrication in the internal combustion engine: an invited review. J Phys, D: Appl Phys 1992;25:A91–A100.
[3] Fitzsimons B. Introduction to the importance of fuel efficiency and role of the ENCYCLOPAEDIC research project, IMechE Seminar: A Drive for Fuel Efficiency, Loughborough, UK; 2011.
[4] Damiani L, Repetto M, Prato AP. Improvement of powertrain efficiency through energy breakdown analysis. Appl Energy 2014;121:252–63.
[5] Morris N, Rahmani R, Rahnejat H, King PD, Fitzsimons B. Tribology of piston compression ring conjunction under transient thermal mixed regime of lubrication. Tribol Int 2013;59:248–58.
[6] Heywood JB. Internal combustion engine fundamentals. Singapore: McGraw-Hill Inc; 1988.
[7] Wang X, Stone CR. A study of combustion, instantaneous heat transfer, and emissions in a spark ignition engine during warm-up. Proc IMechE, Part D: J Automob Eng 2008;222:607–18.
[8] Thangaraja J, Kannan C. Effect of exhaust gas recirculation on advanced diesel combustion and alternate fuels - a review. Appl Energy 2016;180:169–84.
[9] Dehghani Firoozabadi M, Shahbakhti M, Koch CR, Jazayeri SA. Thermodynamic control-oriented modeling of cycle-to-cycle exhaust gas temperature in an HCCI engine. Appl Energy 2013;110:236–43.
[10] Razmara M, Bidarvatan M, Shahbakhti M, Robinett III RD. Optimal exergy-based control of internal combustion engines. Appl Energy 2016;183:1389–403.
[11] Morris N, Rahmani R, Rahnejat H, King PD, Fitzsimons B. The influence of piston ring geometry and topography on friction. Proc IMechE, Part J: J. Eng Tribol 2013;227:141–53.
[12] Tian T, Noordzij LB, Wong VW, Heywood JB. Modelling piston-ring dynamics, blowby, and ring-twist effects. Trans ASME, J Eng Gas Turb Power 1998;120:843–54.
[13] Baker CE, Theodossiades S, Rahnejat H, Fitzsimons B. Influence of in-plane dynamics of thin compression rings on friction in internal combustion engines. Trans ASME, J Eng Gas Turb Power 2012;134:092801–11.
[14] Arcoumanis C, Duszynski M, Flora H, Ostovar P. Development of a piston-ring lubrication test-rig and investigation of boundary conditions for modelling lubricant film properties. SAE Technical Paper No. 952468; 1995.
[15] Han D-C, Lee J-S. Analysis of the piston ring lubrication with a new boundary condition. Tribol Int 1998;31:753–60.
[16] Priest M, Dowson D, Taylor CM. Theoretical modelling of cavitation in piston ring lubrication. Proc IMechE, Part C: J Mech Eng Sci 2000;214:435–47.
[17] Sawicki J, Yu B. Analytical solution of piston ring lubrication using mass conserving cavitation algorithm. Tribol Trans 2000;43:419–26.
[18] Shahmohamadi H, Rahmani R, Rahnejat H, Garner CP, King PD. Thermo-mixed hydrodynamics of piston compression ring conjunction. Tribol Lett 2013;51(3):323–40.
[19] Hu Y, Cheng HS, Arai T, Kobayashi Y, Aoyama S. Numerical simulation of piston ring in mixed lubrication – a nonaxisymmetrical analysis. Trans ASME, J Tribol 1994;116:470–8.
[20] Ma M-T, Smith EH, Sherrington I. Analysis of lubrication and friction for a complete piston-ring pack with an improved oil availability model – part 1: circumferentially uniform film. Proc IMechE, Part J: J Eng Tribol 1997;211:1–15.
[21] Rahmani R, Theodossiades S, Rahnejat H, Fitzsimons B. Transient elastohydrodynamic lubrication of rough new or worn piston compression ring conjunction with an out-of-round cylinder bore. Proc IMechE, Part J: J Eng Tribol 2012;226:284–305.
[22] Michail SK, Barber GC. The effects of roughness on piston ring lubrication – part I: model development. Tribol Trans 1995;38:19–26.
[23] Michail SK, Barber GC. The effects of roughness on piston ring lubrication – Part II: the relationship between cylinder wall surface topography and oil film thickness. Tribol Trans 1995;38:173–7.
[24] Bolander NW, Steenwyk BD, Sadeghi F, Gerber GR. Lubrication regime transitions at the piston ring–cylinder liner interface. Proc IMechE, Part J: J Eng Tribol 2005;219:19–31.
[25] Bolander NW, Sadeghi F. Deterministic modeling of honed cylinder liner friction. Tribol Trans 2007;50:248–56.
[26] Ma Z, Henein NA, Bryzik W. A model for wear and friction in cylinder liners and piston rings. Tribol Trans 2006;49:315–27.
[27] Richardson DE, Borman GL. Theoretical and experimental investigations of oil films for application to piston ring lubrication. SAE Technical Paper No. 922341; 1992.
[28] Mufti RA, Priest M, Chittenden RJ. Analysis of piston assembly friction using the indicated mean effective pressure experimental method to validate mathematical models. Proc IMechE, Part D: J Automob Eng 2008;222:1441–57.
[29] Di Battista D, Cipollone R. Experimental and numerical assessment of methods to reduce warm up time of engine lubricant oil. Appl Energy 2016;162:570–80.
[30] Wang Y, Liang X, Shu G, Wang X, Bao J, Liu C. Effect of lubricating oil additive package on the characterization of diesel particles. Appl Energy 2014;136:682–91.
[31] Rahnejat H. Multi-body dynamics: vehicles, machines and mechanisms. Bury St Edmunds: Professional Engineering Publishing; 1998.
[32] Christopherson DG. A new mathematical method for the solution of film lubrication problems. Proc IMechE 1941;146(1):126–35.
[33] Elrod HG. A cavitation algorithm. Trans ASME, J Lubr Technol 1981;103:350–4.
[34] Dowson D, Higginson GR. Elastohydrodynamic lubrication. Oxford, UK: Pergamon Press; 1966.
[35] Yang P, Cui J, Jin ZM, Dowson D. Transient elastohydrodynamic analysis of elliptical contacts; Part 2: thermal and Newtonian lubricant solution. Proc IMechE, Part J: J Eng Tribol 2005;219:187–200.
[36] Houpert L. New results of traction force calculations in elastohydrodynamic contacts. J Tribol 1985;107(2):241–8.
[37] Mishra PC, Balakrishnan S, Rahnejat H. Tribology of compression ring-to-cylinder contact at reversal. Proc IMechE Part J: J Eng Tribol 2008;222(7):815–26.
[38] Littlefair B, De la Cruz M, Theodossiades S, Mills R, Howell-Smith S, Rahnejat H, et al. Transient tribo-dynamics of thermo-elastic compliant high-performance piston skirts. Tribol Lett 2014;53(1):51–70.
[39] Greenwood JA, Tripp JH. The contact of two nominally flat rough surfaces. Proc IMechE 1971;185:625–34.
[40] Gore M, Perera M, Styles G, King PD, Rahnejat H. Wear characteristics of advanced honed and cross-hatched coated cylinder liners. In: Proceedings of the 66th Annual Meeting and Exhibition of the STLE; 2011. p. 73.
[41] Arcoumanis C, Ostovar P, Mortimer R. Mixed lubrication modelling of Newtonian and shear thinning liquids in a piston-ring configuration. SAE Technical Paper No. 972924; 1997.
[42] Gohar R, Rahnejat H. Fundamentals of tribology. 2nd ed. Imperial College Press; 2012.
[43] Baker C, Rahmani R, Karagiannis I, Theodossiades S, Rahnejat H, Frendt A. Effect of compression ring elastodynamics behaviour upon blowby and power loss. SAE Technical Paper No. 2014-01-1669.
[44] Briscoe BJ, Evans DCB. The shear properties of Langmuir-Blodgett layers. Proc Roy Soc, Ser A: Math Phys Sci 1982;380:389–407.
[45] Styles G, Rahmani R, Rahnejat H, Fitzsimons B. In-cycle and life-time friction transience in piston ring-liner conjunction under mixed regime of lubrication. Int J Engine Res 2014;15(7):826–78.
[46] Sui PC, Ariga S. Piston ring pack friction and lubrication analysis of an automotive engine using a mixed lubrication model. SAE Technical Paper No. 931937; 1993.
[47] Hoffmann KA, Chiang ST. Computational fluid dynamics for engineers. Vol. I., Engineering Education System, Wichita, KS, USA; 1993.
[48] Barlow TJ, Latham S, McCrae IS, Boulter PG. A reference book of driving cycles for use in the measurement of road vehicle emission. Published Project Report PRP354, available through <www.gov.uk>.

[49] Shin K, Tateishi Y, Furuhama S. Measurement of oil-film-thickness between piston ring and cylinder. SAE Technical Paper No. 830068; 1993.
[50] Mufti RA, Priest M. Experimental evaluation of piston-assembly friction under motored and fired conditions in a gasoline engine. J Tribol, Trans ASME 2005;127:826–36.
[51] Rakapoulos CD, Kosmadakis GM, Pariotis EG. Critical evaluation of current heat transfer models used in CFD in-cylinder engine simulations and establishment of a comprehensive wall-function formulation. Appl Energy 2010;87:1612–30.
[52] Irimescu A, Merola SS, Tornatore C, Valentino G. Development of a semi-empirical convective heat transfer correlation based on thermodynamic and optical measurements in a spark ignition engine. Appl Energy 2015;157:777–88.
[53] Molina S, Guardiola C, Martin J, Garcia-Sarmiento D. Development of a control-oriented model to optimise fuel consumption and NOx emissions in a DI Diesel engine. Appl Energy 2014;119:405–16.
[54] Asprion J, Chinellato O, Guzzella L. A fast and accurate physics-based model for the NOx emissions of Diesel engines. Appl Energy 2013;103:221–33.